BEILSTEIN JOURNAL OF NANOTECHNOLOGY

Numerical analysis of vibration modes of a qPlus sensor with a long tip

Kebei Chen‡[1,2,3], Zhenghui Liu‡[2,3], Yuchen Xie[2], Chunyu Zhang[2,3], Gengzhao Xu*[2,3], Wentao Song*[2,3] and Ke Xu[2,3]

Full Research Paper

Open Access

Address:
[1]School of Nano Technology and Nano Bionics, University of Science and Technology of China, Suzhou 215123, China, [2]Platform for Characterization and Test, Suzhou Institute of Nano-Tech and Nano-Bionics, Chinese Academy of Sciences (CAS), Suzhou 215123, China and [3]CAS Key Laboratory of Nanophotonic Materials and Devices, Suzhou Institute of Nano-Tech and Nano-Bionics, Suzhou 215123, China

Email:
Gengzhao Xu* - gzxu2010@sinano.ac.cn;
Wentao Song* - wtsong2017@sinano.ac.cn

* Corresponding author ‡ Equal contributors

Keywords:
finite element method; long tilted tip; noncontact atomic force microscopy; qPlus sensor; quartz tuning fork; simulations

Beilstein J. Nanotechnol. **2021,** *12,* 82–92.
https://doi.org/10.3762/bjnano.12.7

Received: 19 August 2020
Accepted: 20 December 2020
Published: 21 January 2021

Associate Editor: J. Frommer

Abstract

We study the oscillatory behavior of qPlus sensors with a long tilted tip by means of finite element simulations. The vibration modes of a qPlus sensor with a long tip are quite different from those of a cantilever with a short tip. Flexural vibration of the tungsten tip will occur. The tip can no longer be considered as a rigid body that moves with the prong of the tuning fork. Instead, it oscillates both horizontally and vertically. The vibration characteristics of qPlus sensors with different tip sizes were studied. An optimized tip size was derived from obtained values of tip amplitude, ratio between vertical and lateral amplitude components, output current, and quality factor. For high spatial resolution the optimal diameter was found to be 0.1 mm.

Introduction

Quartz tuning forks are widely used in the watch industry because of their low frequency offset over a wide temperature range [1]. In addition, quartz tuning forks have a high elastic constant, a high quality factor (Q factor), and are self-sensing due to the piezoelectric effect [1]. Therefore, a quartz tuning fork can be used as a force sensor. The central part of the "qPlus sensor" is a quartz tuning fork of which one prong is fixed onto a substrate and the other prong with an attached tip serves as a self-sensing cantilever [2]. In 1996, F. J. Giessibl et al. first used the qPlus sensor to measure the morphology of a grating

and a CD at room temperature [3]. Since then, this technique has been used extensively in the fields of physics, chemistry, and materials science to obtain images of high spatial resolution [4-12].

Most research under low-temperature and ultrahigh-vacuum (LT-UHV) conditions has been carried out using the first-order eigenmode of the qPlus sensor, which has a short tip that can be considered as a rigid body vertically attached to the tuning fork prong. However, soft biological samples, such as living cells and lipid membranes [13-15], must be immersed in a liquid environment to maintain their original properties. In order to avoid immersion of the tuning fork and the wiring in the liquid, a longer tip is required. By keeping the nodes of the tip in the higher-order modes close to the liquid surface, the frequency drift of the sensor can be effectively limited, maintaining a high Q factor [16,17]. By using a qPlus sensor with a long tip, atomic resolution and near-field optical images were obtained in liquid environments [15,18,19].

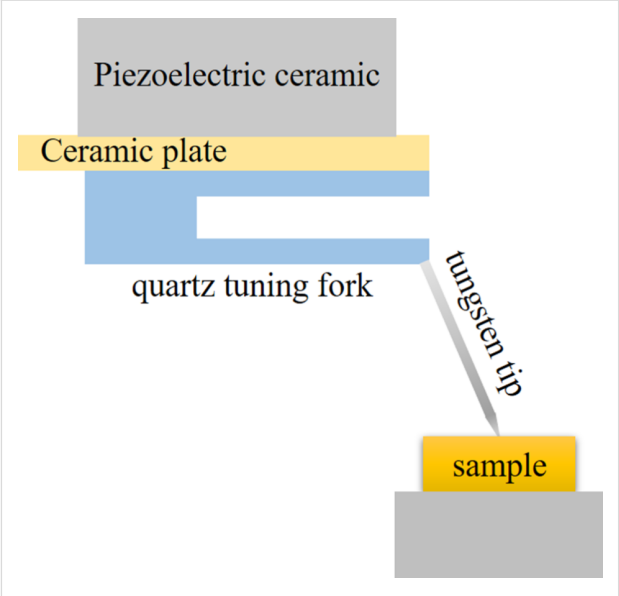

Figure 1: Schematic diagram of a qPlus sensor with a long tilted tip.

For some applications, it is required that the tip is not perpendicular to the prong of the tuning fork [20,21]. The advantage of a qPlus sensor with a long tilted tip (Figure 1) is that forces in multiple directions can be detected due to the multi-directional vibration of the tip [17]. Furthermore, by using a qPlus sensor with a long tilted tip, vertical incident light can be coupled to the tip apex. This setup has the added benefit of locating the exact target location with high resolution when it is combined with an optical microscope to observe the sample surface from upside [22,23]. However, there is only scarce work regarding the analysis of how the shape of the long tilted tip affects the vibration of the sensor. The selection of tip length and diameter often depends on the experience of researchers.

Here, we report a numerical study of the vibration modes of qPlus sensors. Eigenfrequencies, tip amplitudes, ratios between vertical and lateral amplitude components, output currents, and Q factor values as functions of the tip size of the qPlus sensor are systematically analyzed. Eventually, the optimal tip size can be derived from the simulation results.

Methods

Model and parameters

The model in the simulation is based on an MS1V-T1K-type quartz tuning fork used in our experiment (details will be described later). The dimensions of the MS1V-T1K quartz tuning fork, length L = 3423 μm, width W = 687 μm, and thickness τ = 121 μm, are used in the finite element model. The arrangement of the gold electrodes on the tuning fork is the same as in reality. One electrode pair is grounded and the other is set to a virtual ground. The calculated mechanical eigenfrequency of the bare tuning fork is 32.19 kHz. After considering the electrostatic and piezoelectric effects, the eigenfrequency is shifted to 32.23 kHz, which is only 0.12% higher. Therefore, the effect of the shunt capacitance of the tuning fork is negligible.

As shown in Figure 2a, the tungsten tip is attached to one prong using a rectangular drop of Torr seal epoxy. The diameter values of the tungsten tip used in the simulations were chosen according to diameters of the tungsten wire available [24]. We selected four different diameters: 0.025 mm, 0.05 mm, 0.075 mm, and 0.1 mm. The tip length can be customized according to the experimental needs. In this paper, nine lengths are selected for calculation at each diameter: 0.5 mm, 0.65 mm, 0.8 mm, 1.0 mm, 1.2 mm, 1.4 mm, 1.5 mm, 1.7 mm, and 2 mm. The angle between the tip and the prong is 65°. An external excitation is applied by exerting a harmonic displacement of 4.5 nm on the side of the tuning fork prong without a tip. Figure 2b visualizes the mesh distribution used for the calculations. The mesh density increases at the link between the two prongs and near the boundaries of each material. Figure 2c is a zoomed view of the tungsten wire attached to the end of the tuning fork. The epoxy glue is defined as a cuboid in order to facilitate mesh generation and reduce calculation time, since it is not guaranteed to have a fixed geometry after curing. The glue thickness in the simulation is set to be the average glue thickness of the qPlus sensor used in our experiment. In this case, the volume of the glue in the simulation is approximately equal to the volume of the glue in the experiment. Figure 2d is a false-color representation of the total displacement levels. Warmer colors represent a larger displacement.

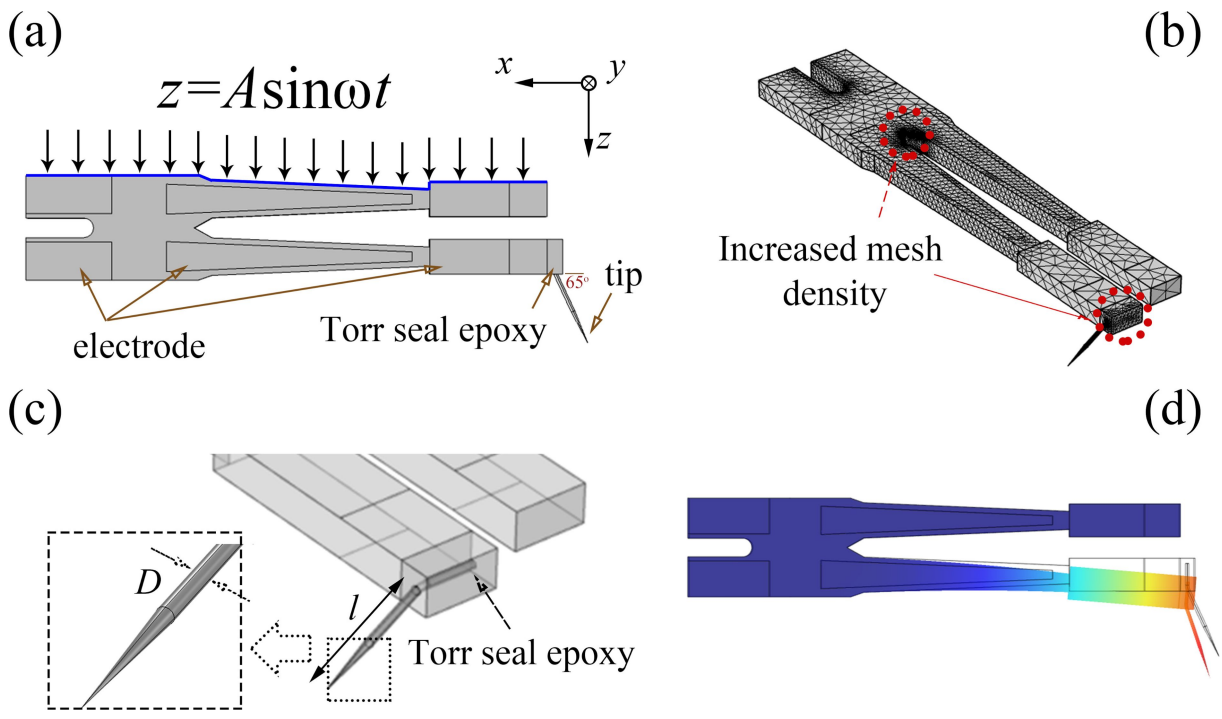

Figure 2: (a) Schematic diagram of the simulation model including tuning fork, Torr seal epoxy glue, and tungsten tip. Mechanical vibration excitation is applied on one side of the tuning fork. (b) Map of the mesh distribution as implemented in the finite element simulation. (c) Zoomed-in view of the tungsten wire attached to the end of the tuning fork. (d) False-color representation of the total displacement levels when the free prong deforms under excitation.

All calculations were carried out using COMSOL Multiphysics. Table 1 summarizes the parameters used, including Young's modulus, Poisson's ratio, mass density, and damping coefficients for all materials considered. The values for Torr seal epoxy were chosen as in the papers by Dennis van Vörden et al. [25] and Omur E. Dagdeviren and co-workers [26]. The parameters for quartz, gold, and tungsten were taken from the materials library of the simulation software, except for the damping coefficient for quartz, which was chosen based on our experimental results. According to [26], it is also worth noting that (i) due to the comparatively low internal damping occurring inside gold and tungsten, we did not assign a damping coefficient to any of these materials to reduce the computational cost, and that (ii) the sensor is oscillating in vacuum.

Observation by scanning electron microscope (SEM)

Firstly, in this paper, the whole assembly consisting of tuning fork, tip, and Torr seal epoxy is referred to as the qPlus sensor. The oscillation of the qPlus sensor with a long tilted tip was experimentally observed using a commercial SEM (FEI Quanta FEG 250). The tungsten wire (Alfa Aesar company) used in the experiment had a diameter of 0.025 mm (0.001 in) and a purity of 99.95%. The tip was obtained by AC electrochemical etching in NaOH solution at a concentration of 1 mol·L^{-1}. A tungsten wire with a length of 942 µm was attached to the end of the tuning fork with Torr seal epoxy. The angle between the tungsten wire and the prong was 65°. The excitation signal was introduced via mechanical excitation of the base part by a piezo

Table 1: Material parameters used for finite element calculations.

Material constant	Quartz	Torr seal epoxy	Gold	Tungsten
Young's modulus (GPa)	78.31	9.39	70	360
Poisson's ratio	0.14	0.45	0.44	0.28
mass density (kg·m^{-3})	2651	1600	19300	19300
damping coefficient	1 × 10^{-4}	5 × 10^{-3}	—	—

actuator. The excitation amplitude was 1 V. The scanning rate of SEM was 20 μs/pixel. The vibration of the qPlus sensor was observed at room temperature while maintaining a pressure of 10^{-3} Pa.

Results and Discussion

Eigenfrequencies and eigenmodes

The eigenfrequencies of three parts are discussed in this paper. These parts are the qPlus sensor, the prong (the free prong of the tuning fork) with one end fixed and the other end carrying a concentrated load which equals the tip mass, and the independent tungsten tip. These three eigenfrequencies are denoted by f_q, f_{tf}, and f_{tip}, respectively. The values of f_q and f_{tip} are obtained by the simulation, and f_{tf} is calculated by the method described in [27]. Since the oscillation of the tip is mainly in the tapping mode during scanning, we focus on the modes of the tuning fork prong and the tip oscillating in the *X*–*Z* plane. We found that when the tuning fork oscillates at the first-order eigenfrequency, there are two different vibration eigenmodes of the tip, as shown in Figure 3a. We name the vibration mode in which the tip and the tuning fork are deflected in the same direction the "in-phase" mode. If the tip and the tuning fork are deflected in opposite directions, we name the corresponding vibration mode the "anti-phase" mode. Figure 3b–e summarizes the relations between f_q and the tip length for the four different tip diameters. In the in-phase mode, the qPlus sensor oscillates at a lower eigenfrequency, and in the anti-phase mode at a higher eigenfrequency. With the increase of tip diameter, the tuning fork shows the vibration of the second-order eigenmode in the anti-phase mode, especially with the shorter tip. This paper does not discuss the second-order eigenmode of the tuning fork, so there are no corresponding frequencies of the anti-phase mode at some tip lengths in Figure 3c–e.

The vibration of the qPlus sensor is the superposition of the oscillation of the tuning fork and the oscillation of the tip. The relations between f_q, f_{tf}, and f_{tip} for the qPlus sensor with a diameter of 0.025 mm tip are shown in Figure 4. The grey dashed lines denote f_{tf}. When the tip length is 0.5 mm, f_q of the in-phase mode is very close to the dashed line (Figure 4a), which means that the tuning fork vibrates in resonance. When f_q moves away from the dashed line and gets closer to f_{tip}, the vibration of the qPlus sensor is mainly dominated by the tip, while the tuning fork hardly oscillates. The value of f_q of the anti-phase mode is close to that of f_{tip} for a 0.5 mm long tip (Figure 4b), resulting in tip resonance. As the tip length increases, f_q gradually approaches f_{tf}, leading to resonance of the tuning fork. If the tip length continues to increase, f_q will be closer to the second-order f_{tip}. The superposition vibration characteristics of the qPlus sensor are reflected in the amplitudes of the tuning fork and the tip, which will be discussed later.

Amplitude of the tuning fork (A_{tfz}) and its output current

In this paper, the amplitude in the *Z* direction of point A on the tuning fork prong in Figure 3a is denoted as A_{tfz}. The amplitude of point B at the tip in Figure 3a is denoted as A_{tip}. A_z and A_x represent the two components of the amplitude of the tip apex in the *Z* and *X* directions, respectively. A_{tip} is equal to $\sqrt{A_x^2 + A_z^2}$. The angle between A_{tip} and A_x is φ. The frequencies near f_q are scanned by the frequency domain study in COMSOL to obtain the maximum values of A_{tfz}, A_x, A_z, and the output currents. Figure 5 shows the A_{tfz} and the simulated output currents.

Rise and drop of A_{tfz} of both modes in Figure 5a–d can be explained by the tuning fork resonance. We take the 0.025 mm tip as an example. When the tip length is 0.5 mm, the tuning fork vibrates resonantly in the in-phase mode (Figure 4a), corresponding to the larger A_{tfz} in Figure 5a. The value of A_{tfz} decreases due to f_q moving far away from f_{tf}. The value of A_{tfz} of the anti-phase mode for a 0.5 mm long tip is small because of the large difference between f_q and f_{tf} (Figure 4b). With the increase of the tip length, f_q gradually gets closer to f_{tf}, and A_{tfz} gradually increases as well. The value of A_{tfz} reaches the maximum value when the tip length is 1.4 mm. At larger tip lengths, f_q gradually moves away from f_{tf}, while A_{tfz} decreases.

Rise and drop of A_{tfz} in both modes are also reflected in the simulated output current. Similar to A_{tfz}, the output current with a shorter tip is larger in the in-phase mode, and the output current with a longer tip is larger in the anti-phase mode (Figure 5e–h). However, we found that the intersection points of the output currents do not coincide with those of A_{tfz} (except for the 0.025 mm tip). For example, when the output current generated in the anti-phase mode is larger than that in the in-phase mode (Figure 5g), the value of A_{tfz} of the anti-phase mode is lower than that of the in-phase mode (Figure 5c). This is because the frequency of the anti-phase mode is higher, that is, the period is shorter. Although the peak value of the charge q of the anti-phase mode, caused by the piezoelectric effect of the tuning fork [1], is smaller than that of the in-phase mode, the maximum value of the partial derivative of q with respect to the time (i.e., the peak output current) can be larger than that of the in-phase mode. The result illustrates that the changes of the output current and of A_{tfz} with respect to the tip length are not necessarily synchronous.

Tip oscillation and SEM observation

Since the tip swings around the end of the tuning fork prong, A_{tip} is different from A_{tfz}. We should focus on the vibration of the tip apex itself. Figure 6 gives A_{tip} and the ratio between A_x and A_z for the four tip diameters with different

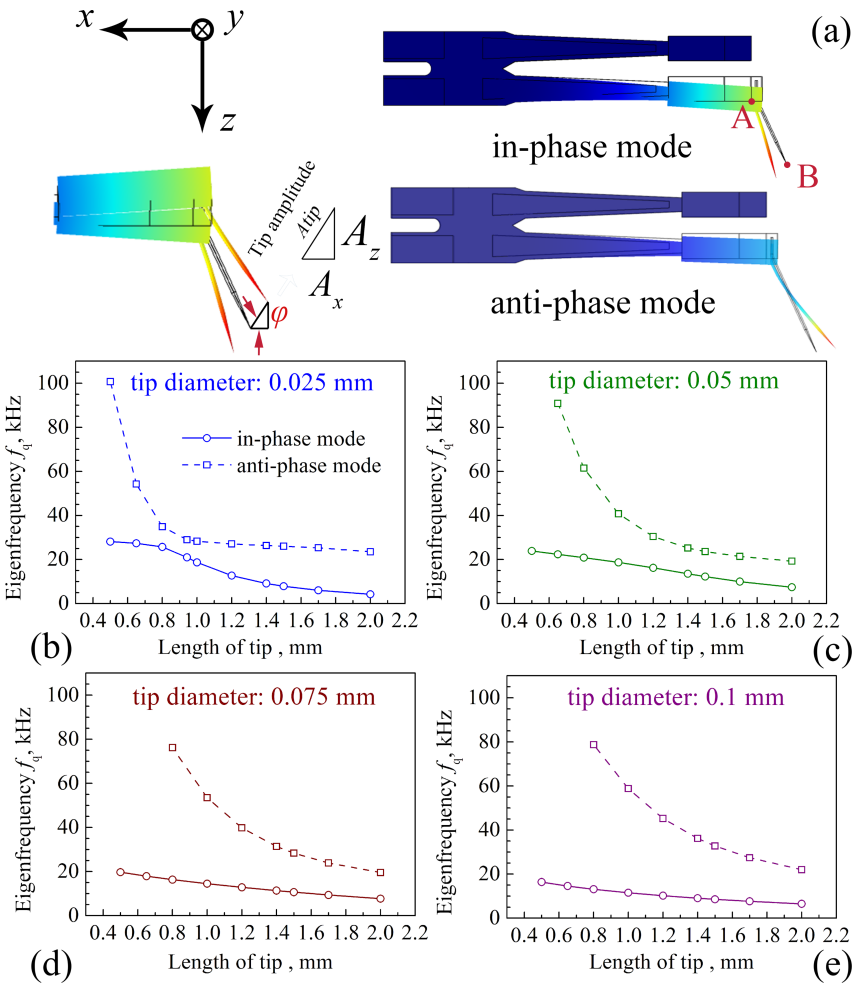

Figure 3: (a) Two different eigenmodes in the simulation. In-phase mode: the tip and the tuning fork deflect in the same direction. Anti-phase mode: the tip and the tuning fork are deflected in the opposite direction. (b–e) The values of f_q of the four tip diameters with different lengths in both eigenmodes.

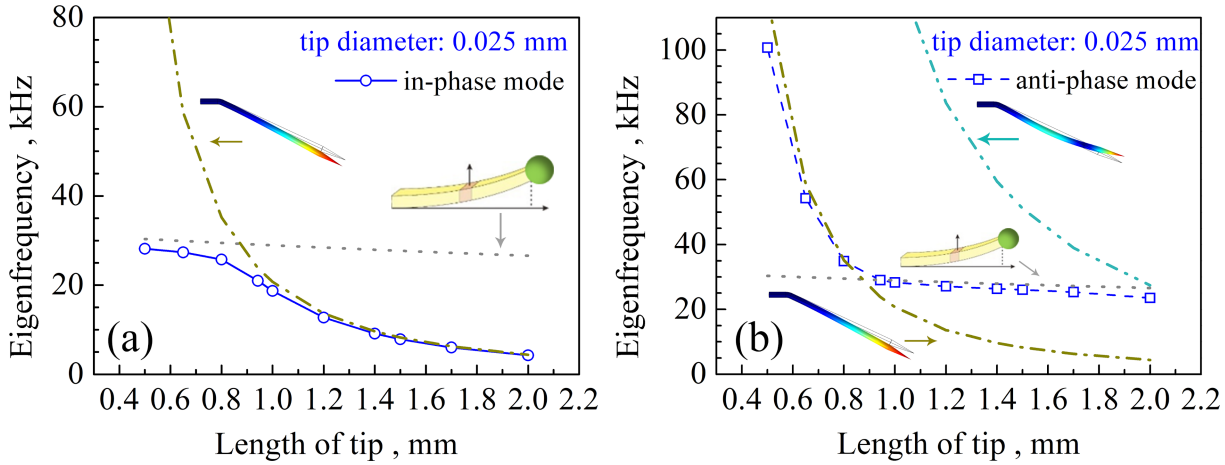

Figure 4: The relations between f_q, f_{tf}, and f_{tip} for the qPlus sensor with a tip diameter of 0.025 mm in the in-phase mode (a) and in the anti-mode (b). The eigenmodes corresponding to f_{tf} and f_{tip} are shown in the illustrations.

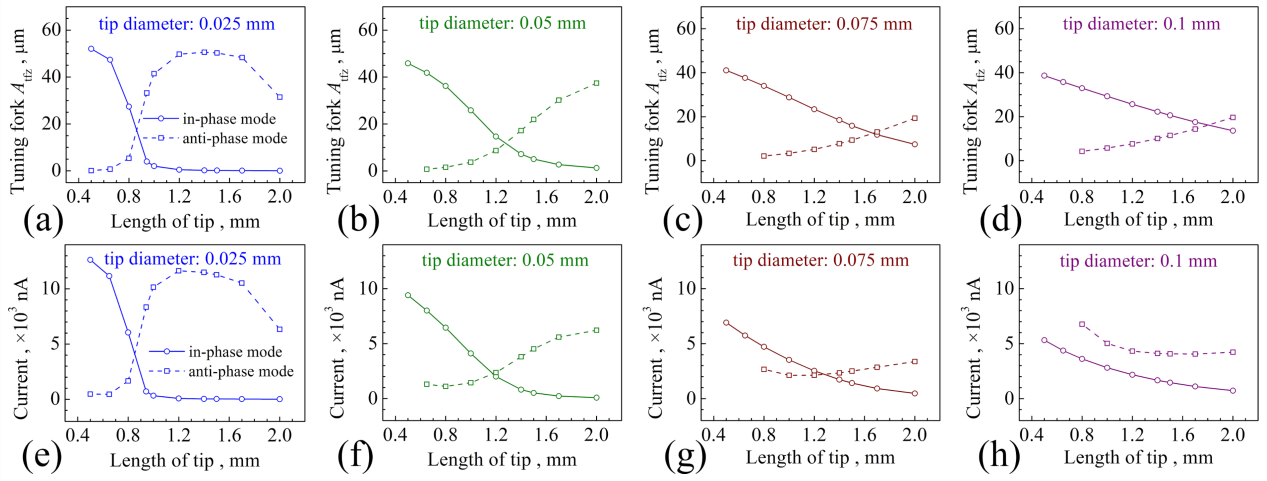

Figure 5: Illustrations of A_{tfz} (a–d) and output currents (e–h) as functions of the tip length for the four different tip diameters.

lengths. We found that for a fixed tip diameter and tip length, A_{tip} is always greater than A_{tfz}. The value of A_x/A_z is the cotangent value of the angle φ (Figure 3a). If $0 < φ < 45°$ then $A_x/A_z > 1$; if $45° < φ < 90°$ then $A_x/A_z < 1$. A higher ratio corresponds to a higher proportion of the oscillation parallel to the X direction. In contrast, a smaller ratio means the tip oscillation is close to the ideal tapping mode. In the in-phase mode, A_x/A_z for all tip diameters increases with respect to the tip length. However, the increase of A_x/A_z is smaller for 0.075 mm and 0.1 mm tips. When the tip gets thinner, the vibration tends to be parallel to the X direction. When the tip gets thicker, the oscillation behaves more like the tapping mode.

The value of A_{tip} is determined through the vibrations of the tuning fork prong and the tip. Therefore, the change of A_{tip} cannot be simply analyzed by the method for analyzing A_{tfz}. Again, we take the 0.025 mm tip as an example. The value of f_{tip} of the in-phase mode gets closer to f_q with the increase of the tip length (Figure 4a). Accordingly, the value of A_{tip} shows a constant rise when the tip length varies between 0.5 and 0.8 mm (Figure 6a). When the tip length exceeds 0.8 mm, A_{tfz} is greatly reduced to almost zero (Figure 5a), which means that the tuning fork hardly oscillates. Therefore, A_{tip} is also reduced. In the anti-phase mode, the qPlus sensor vibrates near the first-order f_{tip} when the tip length ranges between 0.5 and 0.8 mm (Figure 4b). A longer tip length leads to a larger A_{tip} (Figure 6a). At the length of 0.942 mm, the tip apex vibrates almost parallel to the X direction. Therefore, A_x/A_z increases greatly (Figure 6e). However, A_{tip} begins to decrease when the tip is longer than 0.942 mm. This is caused by the change of A_{tfz} and the relative position of the node on the tip. The deflection directions of the tuning fork and the tip are opposite in the anti-phase mode. When the tip is longer than 0.8 mm, A_{tfz} increases quickly with respect to the tip length and the node of the tip moves towards the tip apex. Therefore, A_{tip} decreases. At a tip length of 1.4 mm, A_{tip} reaches its minimal value. Because f_q of the anti-phase mode gets much closer to the second-order f_{tip} when the tip length is longer than 1.4 mm, A_{tip} increases at the same time, and the tip apex oscillates parallel to the X direction again, resulting in a corresponding increase of A_x/A_z.

In order to understand the oscillation behavior of the tip more intuitively, a qPlus sensor with a tip length of 942 µm was fabricated and placed in an SEM to observe the vibration, as shown in Figure 7a. We carried out a series of frequency sweep experiments from 18 to 32 kHz in ambient atmosphere. The obtained response curve is plotted in Figure 7b. We found resonance frequencies of 20.64 and 28.51 kHz in the scanning curve, which are close to the frequencies of 20.98 kHz of the in-phase mode and 28.99 kHz of the anti-phase mode, respectively, from the simulation. When we used a driving frequency between 28.62 and 28.78 kHz in the SEM, the resonance frequency of the qPlus sensor was found at 28.71 kHz (Figure 7d), which is slightly higher than that measured in atmosphere due to less air damping. The oscillation of the apex of the tip is presented in the Figure 7c. The value of A_{tip} measured directly from the SEM images was 1.435 µm, A_z and A_x were 0.47 and 1.35 µm, respectively. The ratio between A_x and A_z was 2.85. In the simulation the values were A_z = 18.09 µm, A_x = 110.81 µm, and A_x/A_z = 6.12. One possible reason for the lower value of A_x/A_z in the SEM is the expansion of the epoxy glue from the tuning fork to the tip (Figure 7a). This is confirmed by a further simulation (see Supporting Information File 1).

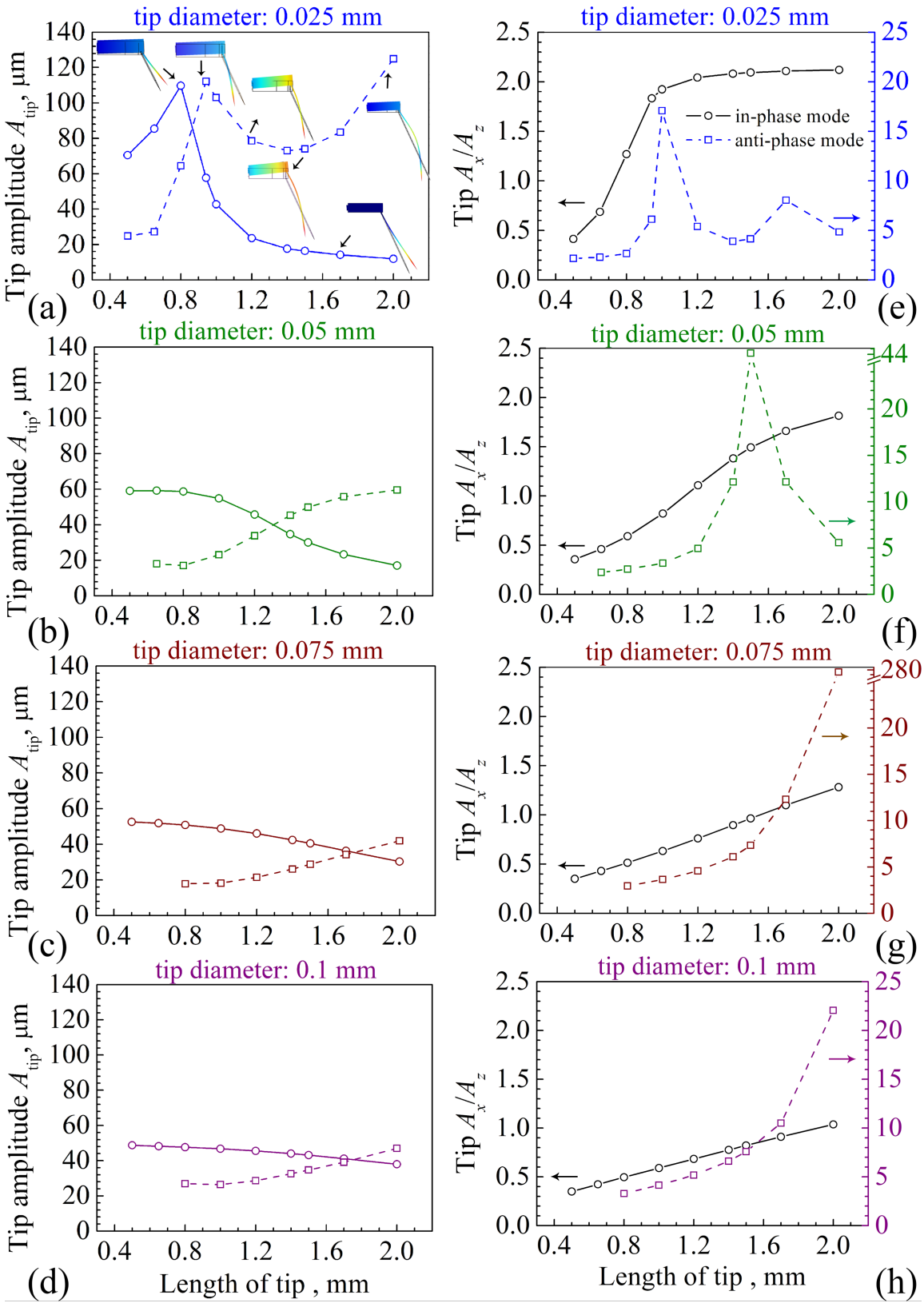

Figure 6: (a–d) A_{tip} and (e–h) A_x/A_z as functions of the tip length depicted for the four different tip diameters. The illustrations in (a) show the oscillation behaviors of the 0.025 mm tip with different lengths in both modes.

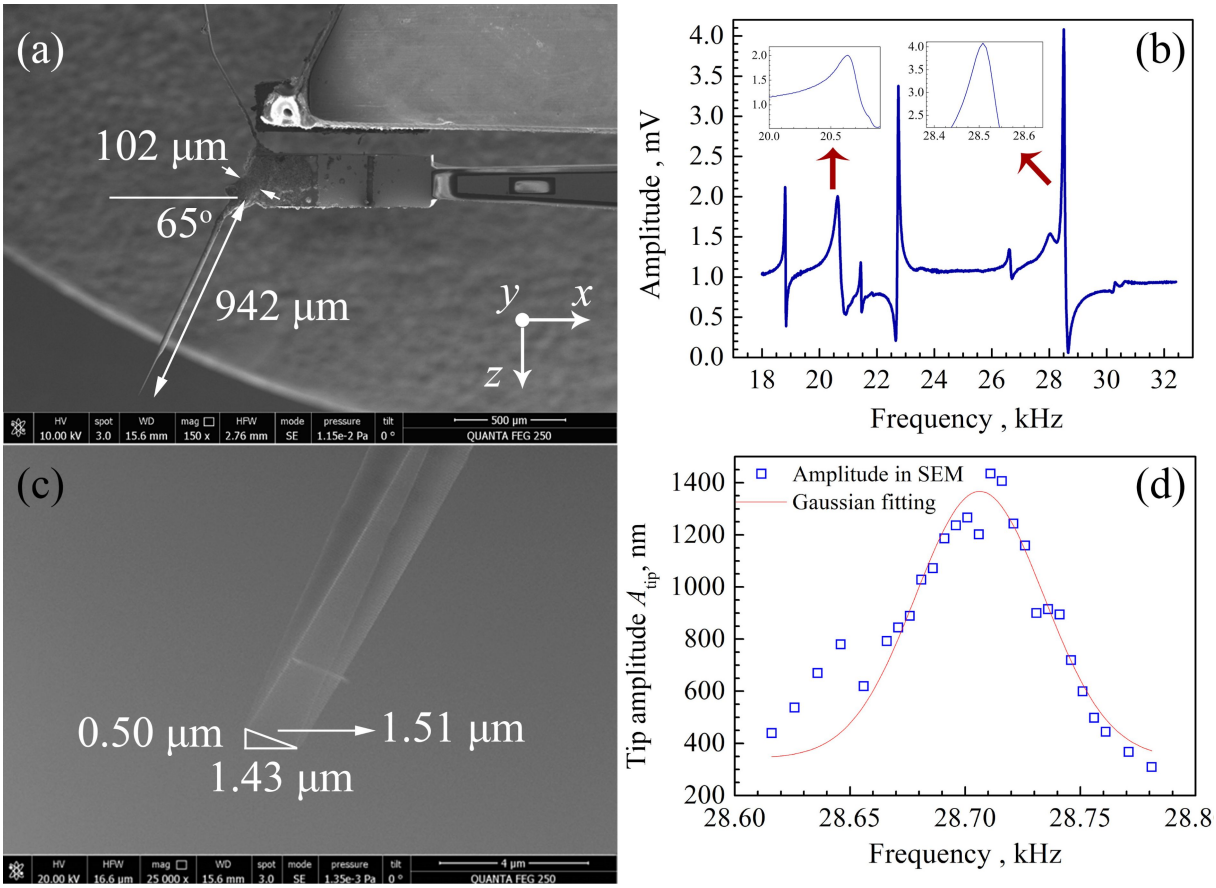

Figure 7: (a) SEM observation of a qPlus sensor with an attached tungsten tip with a length of about 0.942 mm and a diameter of 0.025 mm. (b) Sweeping frequency curve in ambient atmosphere. 20.64 and 28.51 kHz correspond to the values of f_q of the in-phase mode and the anti-phase mode, respectively, from the simulation. (c) Corresponding SEM images taken around the oscillating tip apex. The value of A_{tip} is 1.51 µm, and A_x and A_z are 1.43 and 0.50 µm, respectively. (d) Blue squares: A_{tip} measured from SEM images. Red line: fit with a Gaussian curve. The resonance frequency of 28.71 kHz of the anti-phase mode measured in SEM is slightly higher than that measured in atmosphere due to less air damping.

Tip selection

The purpose of optimizing the tip dimensions is to improve the spatial resolution of the measurement. Therefore, we need to consider all physical parameters comprehensively. Firstly, it is necessary to reduce the influence of the long-range force, where A_{tip} should be small enough. Secondly, f_q should be high to minimize frequency noise [1]. However, there is a tradeoff between A_{tip} and f_q in the in-phase mode (Figure 3 and Figure 6). We found a 0.05 mm tip has the best performance when the tip length is 0.65 mm in the anti-phase mode. However, A_x/A_z in the anti-phase mode is 2.36, that is, φ is 23°. In frequency modulation-atomic force microscopy (FM-AFM), the frequency shift Δf of the cantilever is utilized to detect the forces between tip and sample. The shift Δf induced by the vertical force gradient is tan|φ| times as large as that induced by the lateral force gradient [17]. In other words, in the range from 0 to 90°, if φ > 45°, mainly the vertical force gradient contributes to Δf. If φ < 45°, the lateral force gradient has a greater impact. For most cases, it is desirable to detect a larger vertical force gradient signal, so we need $A_x/A_z < 1$. The in-phase modes were found to fulfil this requirement. Thirdly, we want the stiffness of the qPlus sensor to be large enough to allow for a stable small-amplitude operation [1]. The equivalent stiffness k_{eq} of the qPlus sensor is shown in Figure 8, which is calculated from the strain energy and the tip amplitude with an equivalent point-mass model [28]. We see in Figure 8c that for a 0.075 mm tip, there is an optimal tip length of 2 mm that will achieve the maximum k_{eq}. However, the corresponding vibration is in the anti-phase mode. In the in-phase mode, k_{eq} decreases with the increase of the tip length. When the tip length is longer than 0.65 mm, the value of k_{eq} of the qPlus sensor with 0.1 mm diameter is larger than that of any tip with another diameter. Thus, 0.1 mm would be the best choice for the tip diameter.

The last crucial factor to be considered is the Q factor. Lower Q factors will result in lower stability for both FM-AFM and amplitude modulation AFM (AM-AFM) [17]. As shown in Figure 9, the Q factor of the qPlus sensor is higher for shorter

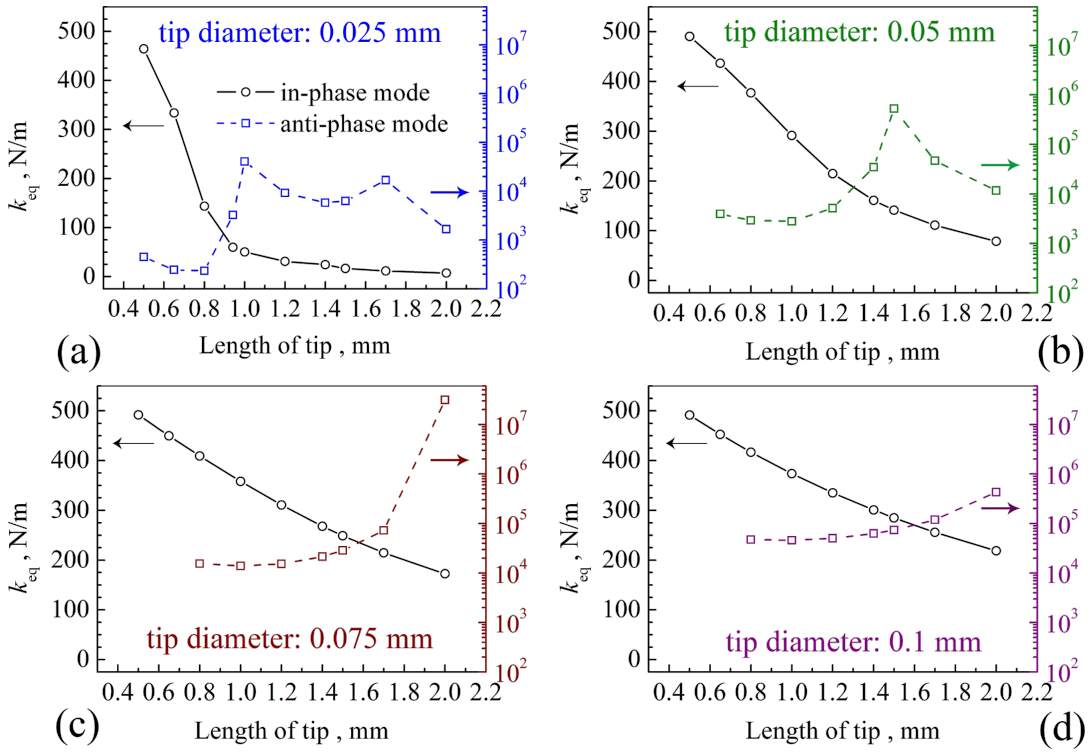

Figure 8: Equivalent stiffness k_{eq} of the qPlus sensor as a function of the tip length depicted for the four different tip diameters.

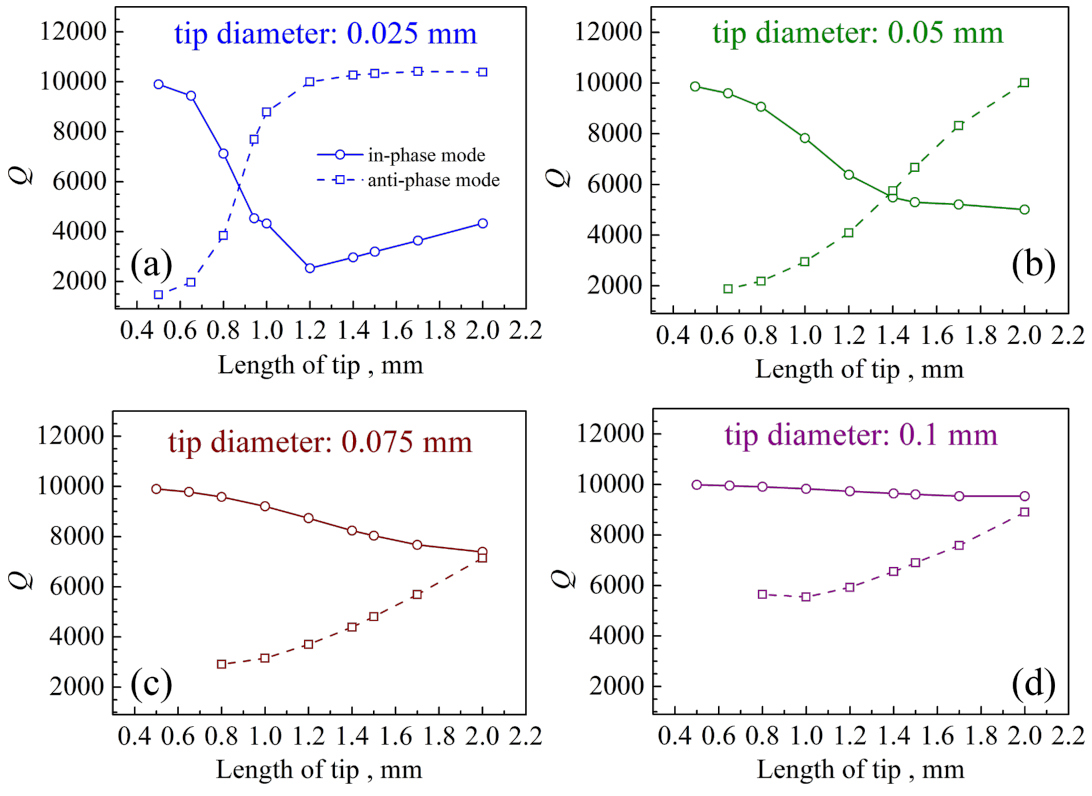

Figure 9: *Q* factor as a function of the tip length depicted for the four different tip diameters.

tips in the in-phase mode. The Q factor of the 0.1 mm tip in the in-phase mode decreases the least when the length increases, and A_{tip} is smallest when the tip length is shorter than 1.2 mm. Therefore, in terms of resolution, a 0.1 mm tip with a length less than 1.2 mm in the in-phase mode would exhibit a better performance.

Conclusion

The oscillation characteristics of qPlus sensors with different dimensions of tungsten tips were studied by using the finite element method. The results reveal that the changes of the output current and the tuning fork amplitude (A_{tfz}) with respect to the tip length are not necessarily synchronous. The tip amplitude (A_{tip}) is determined by vibrations of both the tuning fork prong and the tip. A 0.1 mm tip with a tip length smaller than 1.2 mm used in the in-phase mode can improve the spatial resolution. This research provides quantitative data to optimize the tip dimensions and the corresponding vibration modes of a qPlus sensor with a long tilted tip.

Supporting Information

Supporting Information File 1

Additional simulation results.
[https://www.beilstein-journals.org/bjnano/content/supplementary/2190-4286-12-7-S1.pdf]

Funding

The authors gratefully acknowledge the support from the National Key Technologies R&D Program of China (Grant No. 2016YFA0201101), the National Natural Science Foundation of China (Grants No. 61734008, and No. 11804369), and CAS Pioneer Hundred Talents Program (Song, W.).

ORCID® iDs

Kebei Chen - https://orcid.org/0000-0002-6873-8162
Gengzhao Xu - https://orcid.org/0000-0003-4121-1667

References

1. Giessibl, F. J. Principles and Applications of the qPlus Sensor. In *Noncontact Atomic Force Microscopy: Volume 2;* Morita, S.; Giessibl, F. J.; Wiesendanger, R., Eds.; Springer: Berlin, 2009; pp 122–132. doi:10.1007/978-3-642-01495-6
2. Giessibl, F. J. *Rev. Sci. Instrum.* **2019,** *90,* 011101. doi:10.1063/1.5052264
3. Giessibl, F. J. *Appl. Phys. Lett.* **1998,** *73,* 3956–3958. doi:10.1063/1.122948
4. Hembacher, S.; Giessibl, F. J.; Mannhart, J.; Quate, C. F. *Proc. Natl. Acad. Sci. U. S. A.* **2003,** *100,* 12539–12542. doi:10.1073/pnas.2134173100
5. Emmrich, M.; Huber, F.; Pielmeier, F.; Welker, J.; Hofmann, T.; Schneiderbauer, M.; Meuer, D.; Polesya, S.; Mankovsky, S.; Ködderitzsch, D.; Ebert, H.; Giessibl, F. J. *Science* **2015,** *348,* 308–311. doi:10.1126/science.aaa5329
6. Gross, L.; Mohn, F.; Liljeroth, P.; Repp, J.; Giessibl, F. J.; Meyer, G. *Science* **2009,** *324,* 1428–1431. doi:10.1126/science.1172273
7. Giessibl, F. J. *Appl. Phys. Lett.* **2000,** *76,* 1470–1472. doi:10.1063/1.126067
8. Wastl, D. S.; Weymouth, A. J.; Giessibl, F. J. *ACS Nano* **2014,** *8,* 5233–5239. doi:10.1021/nn501696q
9. Schneiderbauer, M.; Wastl, D.; Giessibl, F. J. *Beilstein J. Nanotechnol.* **2012,** *3,* 174–178. doi:10.3762/bjnano.3.18
10. Pielmeier, F.; Giessibl, F. J. *Phys. Rev. Lett.* **2013,** *110,* 266101. doi:10.1103/physrevlett.110.266101
11. Huff, T. R.; Dienel, T.; Rashidi, M.; Achal, R.; Livadaru, L.; Croshaw, J.; Wolkow, R. A. *ACS Nano* **2019,** *13,* 10566–10575. doi:10.1021/acsnano.9b04653
12. Pawlak, R.; Glatzel, T.; Pichot, V.; Schmidlin, L.; Kawai, S.; Fremy, S.; Spitzer, D.; Meyer, E. *Nano Lett.* **2013,** *13,* 5803–5807. doi:10.1021/nl402243s
13. Koopman, M.; de Bakker, B. I.; Garcia-Parajo, M. F.; van Hulst, N. F. *Appl. Phys. Lett.* **2003,** *83,* 5083–5085. doi:10.1063/1.1634385
14. Rensen, W. H. J.; van Hulst, N. F.; Kämmer, S. B. *Appl. Phys. Lett.* **2000,** *77,* 1557–1559. doi:10.1063/1.1308058
15. Pürckhauer, K.; Weymouth, A. J.; Pfeffer, K.; Kullmann, L.; Mulvihill, E.; Krahn, M. P.; Müller, D. J.; Giessibl, F. J. *Sci. Rep.* **2018,** *8,* 9330. doi:10.1038/s41598-018-27608-6
16. Ichii, T.; Fujimura, M.; Negami, M.; Murase, K.; Sugimura, H. *Jpn. J. Appl. Phys.* **2012,** *51,* 08KB08. doi:10.1143/jjap.51.08kb08
17. Higuchi, S.; Kuramochi, H.; Kubo, O.; Masuda, S.; Shingaya, Y.; Aono, M.; Nakayama, T. *Rev. Sci. Instrum.* **2011,** *82,* 043701. doi:10.1063/1.3569765
18. Kim, S.; Yoo, H.; Lee, K.; Friedman, B.; Gaspar, M. A.; Levicky, R. *Appl. Phys. Lett.* **2005,** *86,* 153506. doi:10.1063/1.1904713
19. Kwon, S.; Jeong, S.; Kang, Y. *Rev. Sci. Instrum.* **2011,** *82,* 043707. doi:10.1063/1.3582662
20. Cinar, E.; Sahin, F.; Yablon, D. *Beilstein J. Nanotechnol.* **2015,** *6,* 2015–2027. doi:10.3762/bjnano.6.205
21. Higuchi, S.; Kubo, O.; Kuramochi, H.; Aono, M.; Nakayama, T. *Nanotechnology* **2011,** *22,* 285205. doi:10.1088/0957-4484/22/28/285205
22. Sapozhnikov, I.; Gorbenko, O.; Felshtyn, M.; Zhukov, M.; Golubok, A. *AIP Conf. Proc.* **2019,** *2064,* 020003. doi:10.1063/1.5087659
23. Guo, T.; Wang, S.; Dorantes-Gonzalez, D. J.; Chen, J.; Fu, X.; Hu, X. *Sensors* **2011,** *12,* 175–188. doi:10.3390/s120100175
24. Thermo Fisher Scientific Ltd. Tungsten wire MSDS. https://chemicals.thermofisher.cn (accessed July 9, 2018).
25. van Vörden, D.; Lange, M.; Schmuck, M.; Schmidt, N.; Möller, R. *Beilstein J. Nanotechnol.* **2012,** *3,* 809–816. doi:10.3762/bjnano.3.90
26. Dagdeviren, O. E.; Schwarz, U. D. *Beilstein J. Nanotechnol.* **2017,** *8,* 657–666. doi:10.3762/bjnano.8.70
27. Thomson, W. T.; Dahleh, M. D. Euler Equation for Beams. In *Theory of Vibration with Applications;* Stenquist, W., Ed.; Prentice Hall: Upper Saddle River, U.S., 1998; pp 271–273.
28. Melcher, J.; Hu, S.; Raman, A. *Appl. Phys. Lett.* **2007,** *91,* 053101. doi:10.1063/1.2767173